

Reconstruction of Mediterranean coastal sea level at different timescales based on tide gauge records

Jorge Ramos Alcántara^{1,2}, Damià Gomis¹, Gabriel Jordà²

¹Institut Mediterrani d'Estudis Avançats (IMEDEA, University of the Balearic Islands – CSIC). Esporles (Mallorca), 07190,
5 Spain

²Centre Oceanogràfic de Baleares, C.N. Instituto Español de Oceanografía (CSIC), Palma de Mallorca, 07015, Spain

Correspondence to: Jorge Ramos Alcántara (jorge.ramos@ieo.csic.es)

Abstract. A coastal sea level reconstruction based on tide gauge observations is developed and applied to the western basin of the Mediterranean sea. The reconstructions are carried out in four frequency bands and are based on an optimal interpolation method in which the correlation between tide gauge data and all coastal points has been determined from the outputs of a numerical model. The reconstructions for frequencies lower than 1 month use monthly observations from the PSMSL database and cover the period from 1884 to 2019. For the reconstruction of higher frequencies, hourly observations from the GESLA-2 dataset are used, and cover from 1980 to 2015. Total sea level is retrieved with high accuracy from the merging of the different frequency bands. Results of a cross-validation test show that independent tide gauge series are highly correlated with the reconstructions. Moreover, they correlate significantly better with the reconstructions than with altimetry data in all frequency bands, and therefore the reconstruction represents a valuable contribution to the attempts of recovering coastal sea level. The obtained reconstructions allow to characterize the coastal sea level variability, to estimate coastal sea level trends along the entire coastline and to examine the correlation between Western Mediterranean coastal sea level and the main North Atlantic climate indices. The limitations and applicability of the method to other regions are also discussed.

1 Introduction

The coastal zone is a fragile region exposed to sea level variations at different time scales. On the one hand, climate change-induced mean sea level rise is expected to have a major impact on low elevation coasts. These are mainly socio-economic impacts (forcing millions of people to move inland, or to develop costly coastal protections), although the ecological impacts associated with the alteration of the sediment budget in coastal regions could also be important (FitzGerald et al., 2008; Kirwan et al., 2010). On the other hand, rapid variations in sea level associated with extreme events (tsunamis, meteotsunamis or storm surges) can also have devastating effects in coastal regions. Climate models project increases in the frequency of some extreme events, which will in any case intensify their impacts as a result of rising mean sea level (Spalding et al., 2014).

In the particular case of southern Europe, a large part of the economy depends on coastal activities. Therefore, it is expected that mean sea-level rise and its associated hazards will have significant impacts on the Mediterranean coasts (Wolff et al., 2018). These impacts include coastal erosion, flooding, damage to coastal structures, or saline intrusion in estuaries and aquifers (Jordà et al., 2012; le Cozannet et al., 2017). Sea level changes (whether gradual mean sea level rise or changes in extreme events) and their impacts are not uniform in space, which makes necessary to study their variability at regional scale, and not only at global scale (Lyu et al., 2014). The processes that introduce small-scale variability in sea level are diverse, but they are particularly relevant in coastal areas due to their shallow depth and to the complexity of topography and bathymetry. For example, the continental slope largely decouples the dynamics of the open ocean from that of the coastal region (Woodworth et al., 2019).

40 In order to carry out a proper coastal management (which nowadays include adaptation strategies to climate change) it is compulsory to have oceanographic databases that allow the understanding of the spatial and temporal sea level variability. In addition to global scale sea level drivers such as the increase in the amount of water in the oceans due to continental ice melting or the thermal expansion, at regional scale there are other key drivers such as the meteorological component (forcing of atmospheric pressure and wind; Gomis et al., 2012) or the coastal circulation. These have a spatio-temporal variability
45 that is not always captured by the current observational networks and some additional information is required (i.e., running ocean barotropic models forced with the available atmospheric pressure and wind reanalyses, in order to resolve the small scales not captured by the sea-level network; Carrère and Lyard, 2003). The study of extreme sea levels is also particularly important due to the impact of these events. Extreme sea levels are caused by different processes and forcings, some of which may vary in intensity and frequency over time (Tsimpis and Shaw, 2010).

50 A first source of sea level observations are tide gauges, which cover different time periods (few records are available before 1960, but there are also series dating back to the 17th century). Whereas tide gauges generally provide very accurate measurements (Douglas, 2001), their main limitation is that they are point-wise measurements with a heterogeneous spatial and temporal distribution. Furthermore, for climate studies it must be taken into account that their measurements are affected by the vertical motion of the ground where they are anchored (Cipollini et al., 2017), which makes necessary to have
55 accurate local estimates of vertical land motion in order to isolate the marine contribution of tide gauge records (Marcos et al., 2019).

60 Since 1992, sea level measurements provided by satellite altimetry are also available. This technique has a global coverage, and by minimising all sources of error affecting the measurements, accuracy close to 1 cm can be achieved (Cazenave et al., 2018). However, altimetric measurements in coastal regions are particularly complex; despite the advances reached in recent years, standard altimetric data are only available from 5–10 km offshore (Marcos et al., 2019; Vignudelli et al., 2019). Altimetric products have also limited spatial and temporal resolution: the separation between adjacent satellite ground tracks is between 50 and 300 km, and the revisiting time is between a few days and a few weeks (Marcos et al., 2019).

65 In addition to the observations described above, in the Mediterranean region there are also some sea level reconstructions based on different data sources that have allowed to deepen the understanding of sea level variability in the region. Thus, Holgate and Woodworth (2004) produced direct estimations of regional trends by averaging tide gauge series. Others (e.g. Tsimpis et al., 2008; Calafat and Gomis, 2009; Meyssignac et al., 2011) combined data from tide gauges, altimetry and numerical model outputs following the reduced space optimal interpolation methodology proposed by Kaplan et al., (1997). However, all these reconstructions focused on the variability of the open ocean and they have neither the spatial resolution
70 nor the temporal resolution required to characterise coastal processes.

This paper presents a sea level reconstruction for the Western Mediterranean coasts that meets two fundamental requirements: i) it covers all coastal regions; and ii) it has the spatial and temporal resolution required to characterise coastal processes. A cross-validation test will demonstrate that it provides better estimates than coastal altimetry, and therefore that

it represents a valuable contribution to the attempts of recovering coastal sea level. Carrying out the reconstruction for
75 different frequency bands will allow to deepen our knowledge on sea level variability at different time scales down to a daily scale (that is, beyond the temporal resolution of previous reconstructions). The methodology followed to obtain the coastal sea level reconstruction is based on the optimal interpolation method (Bretherton et al., 1976; Pedder, 1993); this methodology also provides error estimations, which is essential in this type of reconstructions.

The paper is organized as follows: first, Sect. 2 overviews the different datasets used along this work. Section 3 reviews
80 the optimal interpolation method, detailing how it has been adapted to reconstruct sea level in different frequency bands; the different validation methods used to evaluate the accuracy of the reconstructions are also briefly described. In Sect. 4 we present the main results: the reconstructions, both for different frequency bands and for total sea level, altogether with the results of the cross-validation test and an estimate of the interpolation errors. In Sect. 5 the reconstructions are used to infer some aspects of coastal level variability in the western Mediterranean. All results are discussed in Sect. 6, examining the
85 limitations of the method and comparing the reconstructions with coastal altimetry products and open ocean reconstructions. Finally, conclusions are presented in Sect. 7.

2 The data sets

2.1 Tide gauge data

We have used two tide gauge datasets: GESLA–2 (Global Extreme Sea Level Analysis, <https://www.gesla.org/>), which
90 has data with a maximum frequency of 1 hour, and PSMSL (Permanent Service for Mean Sea Level, <https://www.psmsl.org/>), with monthly data. The GESLA database was created from the need to have information on extreme events (in particular on their interannual variability), and in a first version (GESLA–1, which was not published) it collected data from two international banks: UHSLC (University of Hawaii Sea Level Center) and GLOSS 2 (Global Sea Level Observing System), as well as from several national banks. In 2016, with the aim of updating the database and
95 extending its spatial coverage, the GESLA–2 set was published. In this new set, the geographical coverage of some regions (including the Mediterranean Sea) was improved, especially for the second half of the 20th century. GESLA–2 has allowed more globally representative analyses since about 1970 (Woodworth et al., 2016). GESLA–2 has its own quality control: the quality and possible use of each data is specified (Piccioni et al., 2019). In this work, only the measurements marked as "correct" were selected. For the period between 1980 and 2015 and for the western Mediterranean basin, 34 tide gauge
100 records are available (Table 1). Only Cagliari tide gauge series showed an obvious datum shift; this made necessary to visually identify the intervals with different datums and subtract their means separately, in order to convert the original data into zero-mean anomalies.

The PSMSL, managed by the National Oceanography Centre in Liverpool, collects data from numerous institutions around the world. This bank has Revised Local Reference (RLR) series, which are referenced to a common datum, and
105 constitute approximately two thirds of the total number of stations. All the series used in this work are of the RLR type.

Although the PSMSL has some series starting in the late 19th century, the number of stations increases considerably in the second half of the 20th century, concentrating along the most developed coastal regions, especially Europe and North America (Holgate et al., 2013). From the PSMSL, 38 tide gauges were selected from the western Mediterranean basin (Table 2). In this case the reconstruction was carried out from the time when the first tide gauge has monthly measurements, namely 110 the Genoa tide gauge, whose series starts in 1884.

The glacial isostatic adjustment (GIA) has not been applied to the tide gauge series. This correction is rather small in the Mediterranean, except for the Adriatic Sea (Marcos and Tsimplis, 2007a), which is not part of our reconstruction domain.

115 **Table 1: GESLA-2 Tide Gauges in the Western Mediterranean Basin, with their Locations, Start and End Dates of the Series, and the Percentage of Missing Data.**

Station	Latitude	Longitude	First data	Last data	Missing values (%)
Ajaccio	41.92	8.76	1981-07-25	2014-09-22	58.64
Alcudia	39.83	3.14	2009-09-11	2014-12-31	0.52
Algeciras	36.12	-5.43	1980-01-01	2012-12-31	16.43
Almería	36.83	-2.48	2006-01-01	2014-12-31	2.13
Barcelona	41.34	2.16	1993-01-01	2014-12-31	2.05
Cagliari	39.21	9.11	1986-12-17	2010-11-30	19.60
Carloforte	39.15	8.31	1988-06-27	2010-12-01	26.91
Ceuta	35.90	-5.32	1980-01-01	2012-12-31	5.53
Formentera	38.73	1.42	2009-09-25	2014-12-31	1.77
Fos-sur-Mer	43.40	4.89	2006-01-31	2014-09-22	50.17
Gandía	39.00	-0.15	2007-07-06	2014-12-31	1.46
Genova	44.41	8.93	1998-08-06	2010-10-13	2.07
Gibraltar	36.12	-5.35	1980-01-01	2000-04-30	33.45
Ibiza	38.91	1.45	2003-01-01	2014-12-31	1.14
Imperia	43.88	8.02	1986-12-11	2010-10-13	30.60
La Figueirette	43.48	6.93	2011-05-24	2014-12-31	2.43
Mahón	39.89	4.27	2009-10-29	2014-12-31	0.21
Málaga	36.72	-4.42	1980-01-01	2014-12-31	0.38
Marseille	43.30	5.35	1985-01-01	2014-12-31	45.97
Melilla	35.29	-2.92	2007-10-23	2014-12-31	1.07
Monaco Fontvieille	43.73	7.42	1980-12-31	2014-12-31	46.71
Monaco Port Hercule	43.73	7.42	1999-04-15	2010-12-01	1.98
Motril	36.72	-3.52	2005-01-01	2014-12-31	0.25
Nice	43.70	7.29	1981-07-03	2014-12-31	47.45
Palma de Mallorca	39.56	2.64	2009-09-11	2014-12-31	0.15
Port Camargue	43.52	4.13	2009-11-05	2012-12-31	20.56
Port Ferreol	43.36	6.72	2012-03-29	2014-12-31	1.39
Port Vendres	42.52	3.11	1981-12-28	2014-04-02	29.21

Porto Torres	40.84	8.40	1985-05-22	2010-11-30	34.73
Sagunto	39.63	-0.21	2007-06-13	2014-12-31	0.54
Sète	43.40	3.70	1992-01-07	2014-02-07	19.71
Tarifa	36.00	-5.60	1980-01-01	2014-12-31	7.15
Toulon	43.12	5.91	1981-06-28	2014-09-22	33.37
Valencia	39.46	-0.33	1992-10-01	2014-12-31	1.46

Table 2: PSML Tide Gauges in the Western Mediterranean Basin, with their Locations, Start and End Dates of the Series, and the Percentage of Missing Data.

Station	Latitude	Longitude	First data	Last data	Missing values (%)
Ajaccio	41.92	8.76	1981-08-15	2019-06-15	50.33
Alcudia	39.83	3.14	2009-10-15	2018-12-15	1.80
Algeciras	36.12	-5.43	1943-07-15	2018-12-15	19.54
Alicante	38.34	-0.48	1960-01-15	1997-12-15	3.07
Almería	36.83	-2.48	1977-11-15	2018-12-15	24.09
Barcelona	41.34	2.17	1993-01-15	2018-12-15	3.85
Cagliari	39.20	9.17	15/08/1896-08-15	2014-12-15	57.71
Carloforte	39.15	8.31	2001-01-15	2015-12-15	0.00
Cartagena	37.60	-0.97	1977-05-15	1987-11-15	12.60
Ceuta	35.89	-5.32	1944-03-15	2018-12-15	3.23
Formentera	38.73	1.42	2009-10-15	2018-12-15	8.11
Fos-sur-Mer	43.40	4.89	2006-02-15	2019-06-15	34.16
Gandía	39.00	-0.15	2007-07-15	2018-12-15	1.45
Genova	44.40	8.90	15/06/1884-06-15	2014-12-15	21.57
Gibraltar	36.15	-5.36	1961-07-15	2014-05-15	39.84
Ibiza	38.91	1.45	2003-02-15	2018-12-15	1.05
Imperia	43.88	8.02	2001-01-15	2015-12-15	0.00
L'Estartit	42.05	3.21	1990-01-15	2019-06-15	0.00
Mahón	39.89	4.27	2009-11-15	2018-12-15	2.73
Málaga	36.71	-4.42	1944-01-15	2018-12-15	16.44
Marseille	43.28	5.35	15/02/1885-02-15	2019-06-15	6.20
Melilla	35.29	-2.93	2008-01-15	2018-12-15	5.30
Monaco	43.73	7.42	1956-01-15	2019-06-15	48.16
Motril	36.72	-3.52	2005-01-15	2018-12-15	1.19
Nice	43.70	7.29	1978-01-15	2019-06-15	12.65
Palma de Mallorca	39.55	2.62	1964-01-15	2018-12-15	60.76
Port Ferreol	43.36	6.72	2012-04-15	2019-06-15	6.90
Port-la-Nouvelle	43.01	3.06	2013-06-15	2019-06-15	1.37
Port-Vendres	42.52	3.11	1984-01-15	2019-06-15	24.18

			15/08/1896-08-15		
Porto Maurizio	43.87	8.02		1922-07-15	0.96
Porto Torres	40.84	8.40	2001-01-15	2015-12-15	2.22
Sagunto	39.63	-0.21	2007-09-15	2018-12-15	2.94
Sète	43.40	3.70	1992-01-15	2019-06-15	14.85
Tarifa	36.01	-5.60	1943-09-15	2018-12-15	5.64
Tarragona	41.08	1.21	2011-06-15	2018-12-15	1.10
Toulon	43.11	5.91	1961-01-15	2019-06-15	43.45
Valencia	39.44	-0.31	1994-01-15	2018-12-15	2.00
Villa Sanjurjo	35.25	-3.92	1944-01-15	1949-11-15	0.00

120 2.2 SOCIB WMOP model

In order to obtain information on the dynamic relationships between different locations (see Sect. 3), the outputs of the numerical model managed by the Balearic Islands Coastal Observing and Forecasting System (SOCIB) have been used. SOCIB is a multi-platform observatory whose products include numerical model outputs to support operational oceanography. Through a regional configuration of the ROMS model (Shchepetkin and McWilliams, 2005) for the western

125 Mediterranean basin, SOCIB has implemented a forecasting system called WMOP that provides daily forecasts with a 3 days time horizon for temperature, salinity, sea level and currents (Juza et al., 2016). The daily forecasts as well as all model outputs from the moment it was implemented can be downloaded from the SOCIB website (<https://www.socib.es>). For sea level, the spatial resolution of the outputs varies between 1.8 and 2.2 km and they are available every 3–4 hours since August 2013 (Juza et al., 2016). The coastal points of this model grid were used to define the grid for the sea level reconstructions 130 presented later on, as the spatial correlations on which the optimal interpolation method is based were calculated from the model outputs.

2.3 Altimetry data and dynamic atmospheric correction

The European observation programme Copernicus provides, through the Copernicus Marine Environment Monitoring Service (CMEMS), regular and systematic baseline information on the global ocean and European seas. Among others 135 CMEMS delivers sea level products derived from a direct processing of altimetric observations (von Schuckmann et al., 2018). In order to compare the coastal reconstructions obtained in this work with the latest generation of altimetric data, sea level anomalies from multi-mission satellite altimetry products were downloaded from the CMEMS website (product identifier: SEALEVEL_MED_PHY_L4 REP_OBSERVATIONS_008_051, last accessed on 6 May 2021 and now included as part of the SEALEVEL_EUR_PHY_L4_MY_008_068). The processing of this dataset includes some corrections such as 140 the removal of high-frequency variability, implemented to avoid the aliasing that could result from the low spatio-temporal resolution of altimetric observations (Gomis et al., 2012). This correction, called DAC (Dynamic Atmospheric Correction), removes a significant part of the sea level variability associated with the atmospheric component, and therefore had to be

reversed. The DAC is produced by CLS using the Mog2D model from Legos (Carrère and Lyard, 2003) and distributed by Aviso+, with support from CNES (<https://www.aviso.altimetry.fr/en/data/products/auxiliary-products/dynamic-atmospheric-correction/description-atmospheric-corrections.html>). These DAC data were bilinearly interpolated onto the coastal points where altimetric sea level anomalies were available and added to these series.

2.4 Climatic indices

In order to study the relationship between the variability inferred from our coastal sea level reconstructions and large-scale atmospheric modes, climatic indices were downloaded for the four modes that are most relevant for the Western Mediterranean basin: the North Atlantic Oscillation (NAO), the East Atlantic pattern (EA), the East Atlantic/Western Russian (EA/WR) and the Scandinavian pattern (SCAN). The NAO index is the main mode of variability in winter, and accounts for the large-scale variation in atmospheric mass between the areas of the Azores subtropical anticyclone and the low-pressure area near Iceland. The EA index influences the freshwater flux into the north-east Atlantic, and also influences the western Mediterranean basin. The EA/WR index contributes to heat fluxes and has an impact on precipitation in the Mediterranean. The SCAN index is related to the climate of the Scandinavian Peninsula and East Asia, as well as to the precipitation in northern Europe (Bueh and Nakamura, 2007; Josey et al., 2011; Martínez-Asensio et al., 2014). All series were obtained from the NOAA Climate Prediction Centre (<http://www.cpc.ncep.noaa.gov/data/teledoc/telecontents.shtml>) and consist of monthly data covering the period from 1950 to present.

3 Methodology

3.1 Optimal Interpolation

Optimal Interpolation is a type of linear statistical interpolation in which the best representation of the state vector of a system at a given point (ϕ_g) is obtained through the superposition of a first guess at that point (ϕ_g^{fg}) and the weighting of the differences between observed data (ϕ^o) and those estimated by the first guess at each observation point (ϕ_i^{fg}) (Hasselmann et al., 1997):

$$\phi_g = \phi_g^{fg} + W_{gi}(\phi_i^o - \phi_i^{fg}) = \phi_g^{fg} + W_{gi}\phi_i' \quad (1a)$$

where W_{gi} are the weights applied to the differences at each observation point i to obtain the state vector at point g . For a discrete set of m interpolation points, Eq. (1a) can be written as:

$$\phi_g = \phi_g^{fg} + \mathbb{W}\phi' \quad (1b)$$

where ϕ_g and ϕ_g^{fg} are m -vectors, ϕ' is the n -vector of anomalies at the n observation points, and \mathbb{W} is the $m \times n$ weight matrix. The method is named as ‘Optimal Interpolation’ because the weights are determined through the statistical

160 minimisation of the mean square error between the real and the interpolated field. The development of this minimisation leads to the expression:

$$\underline{\phi}_g = \underline{\phi}_g^{fg} + \underline{\theta} \mathbb{T}^T \underline{\phi}' \quad (2)$$

where $\underline{\theta}$ is an $m \times n$ matrix whose elements are correlation values between series at interpolation points and at observation points, and \mathbb{T} is an $n \times n$ matrix whose elements are correlation values between series at observation points.

165 Under the assumption of spatially uncorrelated noise, this has no effect on $\underline{\theta}$, but the diagonal of \mathbb{T} (the correlation of observation series with themselves) includes the noise of the observations. Thus, matrix \mathbb{T} can be expressed in terms of a correlation matrix between true values $\underline{\theta}^o$, the noise-to-signal coefficient (variance of the errors divided by the variance of the signal) of the observations η^2 and the identity matrix \mathbb{I} :

$$\mathbb{T} = \underline{\theta}^o + \eta^2 \mathbb{I} \quad (3)$$

170 where the noise-to-signal coefficient η^2 has been assumed to be the same for all observation points. This method also provides an explicit expression of the interpolation error in a statistical sense. That is, the mean value of the interpolation errors that would result if an infinite number of realizations of the observed field were interpolated in the same way (with the same observation points and the same weights). The errors at each interpolation point (ε_g) is given by (Gomis and Pedder, 2005):

$$175 \quad \varepsilon_g = \sigma_g (1 - \underline{\text{Diag}}_g \underline{\text{Tr}}_g [\underline{\theta}^T \mathbb{T}^T \underline{\theta}]) \quad (4)$$

where σ_g is the variance of the signal at point g , and $\underline{\text{Diag}}_g \underline{\text{Tr}}_g [\bullet]$ denotes the trace element of the diagonal of matrix $[\bullet]$ corresponding to the interpolation point g .

3.2 Implementation and evaluation of the reconstruction methodology

180 The reconstruction has been performed in different frequency bands. The main reason is that spatial correlations may differ for different time scales (e.g., daily variability may have associated shorter spatial scales than multidecadal changes). Thus, the splitting in frequency bands allows a more accurate spatial interpolation. Furthermore, because high-frequency signals usually dominate and mask low frequencies, the separation in frequency bands allows a better representation of low frequencies (e.g., interannual and decadal variability).

185 The monthly PSMSL data were separated into three frequency bands: a first one corresponding to periods longer than 10 years ($T > 10y$), a second one corresponding to periods between 1 and 10 years ($1y < T < 10y$), and a third one corresponding to periods between 1 month and 1 year ($1m < T < 1y$). The GESLA-2 hourly data were first averaged into daily data, and then a

frequency band corresponding to periods between 1 day and 1 month ($1d < T < 1m$) was isolated. The number of stations considered for each frequency band was different (Fig.1) and dependent on the length of the series. Namely:

190 • For the $T > 10y$ band, 5 series with at least 20 years of consecutive data were selected. The frequency band was isolated by means of a low-pass filtering carried out using a Butterworth filter of order 10, subtracting from each series the average of a period in which all of them had data.

• For the band $1y < T < 10y$, tide gauges with at least 10 years of consecutive data were considered (see Fig. 1). First, the reconstruction obtained in the previous step in the nearest grid point to the tide gauge was subtracted from the original series and then the frequencies corresponding to periods $T < 1y$ were removed, also by means of a Butterworth filter of order 10.

195 • For the band $1m < T < 1y$, all available PSMSL tide gauges were considered (see Fig. 1), and the two frequency bands reconstructed in the previous steps were removed from the original series. As these consisted of monthly data, there was no need to remove the periods $T < 1m$.

200 • For the $1d < T < 1m$ band, the three previous reconstructions (obtained from PSMSL data) were subtracted from each of the GESLA-2 series (this required a prior conversion of the three bands to daily values by means of linear interpolation).

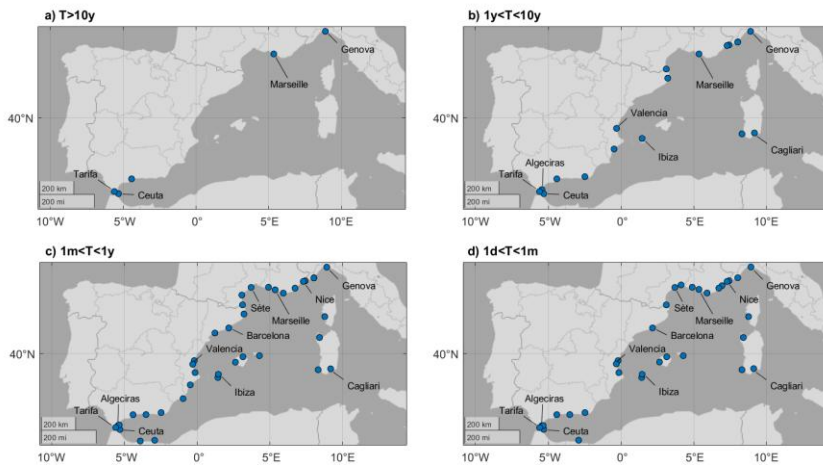


Figure 1: Maps of the tide gauges selected in each band: (a) PSMSL tide gauges used in the reconstruction for the frequency band below 10 years. (b) PSMSL tide gauges used in the reconstruction for the frequency band between 1 and 10 years. (c) PSMSL tide gauges used in the reconstruction for the frequency band between 1 month and 1 year. (d) GESLA-2 tide gauges used in the reconstruction for the frequency band between 1 day and 1 month.

205 The implementation of the optimal interpolation required to estimate the correlations between interpolation points and
 observation points, and also between each pair of observation points. For this purpose, two approaches were followed, one
 based on model data (used to interpolate the frequency bands $1y < T < 10y$, $1m < T < 1y$ and $1d < T < 1m$) and a second one based
 on fitting an analytical correlation function (used to interpolate the band $T > 10y$, for which the period spanned by the model
 does not allow a reliable estimation of correlations). These two approaches are described in the following.

210 • Calculating correlations from numerical model outputs: defining the interpolation points as the coastal points of the
 SOCIB model grid and approximating the location of each tide gauge to the nearest grid point (which implies a
 minimum error given the spatial resolution of the model) makes the calculation of all necessary correlations
 straightforward. The elements of matrices θ and θ^o appearing in Eq. (2) and Eq. (3), which correspond to correlations
 between true values of the field, were computed in this way for the three frequency bands.

215 In order to validate this procedure, the correlations obtained for the pairs of SOCIB model series collocated with tide
 gauges were compared with those obtained for the original tide gauge series. The latter were found to be lower than the
 correlations between model series, due to the presence of observational noise. In order to simulate observations with
 model data, a Gaussian noise was added to the model series closest to the tide gauges, with a variance adjusted to make
 model correlations as close as possible to tide gauge correlations. These model series with added noise were used as
 pseudo-observations to carry out a first test: the optimal interpolation of these pseudo-observations at all coastal points
 220 was compared with the original model series with the aim of verifying the ability of the method to reproduce coastal sea
 level at all locations from a discrete number of observations. For more information on this validation test, see Appendix
 A.

225 • By fitting an analytical correlation function: correlation functions typically depend inversely on distance (e.g., Gaussian
 functions; Rasmussen, 1996). For the 5 tide gauges considered for the frequency band $T > 10y$, the following function
 was used:

$$\theta_{ij} = e^{-\frac{d_{ij}^2}{2L_s^2}} \cdot e^{-\frac{|dt|}{L_t}} \quad (5)$$

230 where d_{ij} represents the distance between locations i and j , and L_s is the characteristic length scale of spatial correlation.
 This was fitted considering the correlations between the 11 tide gauges available in the whole Mediterranean sea with
 long enough time series, resulting in a value of 1254 km. The second part of the expression corresponds to a temporal
 correlation between observations (it is based on the exponential functions typically used to define the weights of
 correlation matrices, see e.g., Pozzi et al., 2012) and is not always used in Optimal Interpolation. In our case, using
 observations from different times intends to compensate for the small number of observations available at a given time;
 namely, we considered observations two years ahead and two years behind the time of each interpolated value,

obviously with weights decreasing with the time distance, dt . The characteristic scale of temporal correlations, L_t , was
235 set to two years.

Another parameter necessary for the implementation of Optimal Interpolation is the noise-to-signal coefficient of
236 observations appearing in Eq. (3). This coefficient was optimised using the golden section search, which is appropriate for
finding the minimum or maximum of unimodal functions through successive reduction of the range of values within which
the extreme is known to exist (Pejic and Arsic, 2019). In our case, we searched for the noise-to-signal coefficient that
240 minimised the mean square error between the original tide gauge series and the reconstructed series through a cross-
validation test that will be explained in the next section.

3.3 Validation of the reconstructions

In order to make a diagnosis of the reconstructions, cross-validation tests were carried out. These tests use part of the
available observations to fit the model, while the other part is used as a validation set (Hastie et al., 2008). In our case, the
245 sea level series at the closest grid points to each tide gauge were obtained considering in each case as observations all
available tide gauges except the one closest to that grid point, which was kept as validation series. The reconstructed series
were then compared with the tide gauge series using several statistics, namely: i) the root mean square error (RMSE),
considered as a standard metric to model errors; ii) the percentage of the variance of observations explained by the
reconstruction; iii) the Pearson correlation coefficient between the reconstructed series and the tide gauge series. This was
250 done for each frequency band in which the reconstructions were carried out.

Another validation test consisted of recovering the original monthly signals from the sum of the first three frequency band
reconstructions, and of the original daily signals from the sum of the four band reconstructions. The comparison of these
unified signals with the original tide gauge series allows to verify that the split into frequency bands has been carried out
255 correctly, and that it is possible to reconstruct the complete series at all interpolation points. From the interpolation errors
calculated for the reconstructions of the different frequency bands, the theoretical interpolation error of the total
reconstruction can also be obtained: assuming that the errors of the reconstructions in the different frequency bands are
independent of each other, the variance of the total error is the quadratic sum of the variances of the error in each band.

Finally, the total reconstructed series, as well as the reconstructed series of each frequency band, were compared with the
last generation of altimetric products and checked against the original tide gauge series, in order to determine the goodness
260 of each approximation.

4 Coastal Reconstruction Validation

4.1 Results of the cross-validation test

In general, the statistics of the cross-validation test described in Sect. 3.3 gave good results when applied to the
reconstructions of the 4 frequency bands (Fig. 2, 3 and 4): most reconstructions explain a high percentage of the variance of

265 the original series and also show good correlations with the original series. The lowest frequency band ($T>10y$) displays the best results: RMS differences are below 2 cm for all tide gauges, and correlations range from a minimum value of 0.74 in Ceuta and a maximum value of 0.99 in Marseille. For this band, the reconstruction explains more than 75 % of the variance of the original series at all stations except in Ceuta, where it only explains 39 %. These results show that a few stations (only 4 in the present case) are enough to reconstruct the low-frequency (decadal) variability, since this is mainly associated with 270 large-scale spatial structures (Woodworth et al., 2019). Considering the observations from the two years before and after each interpolation time has also helped to obtain good estimates.

275 For the interannual to decadal frequency band ($1y < T < 10y$) the reconstructions explain in general smaller percentages of the tide gauge variance than for the other frequency bands. The best results are obtained at the stations located on the east coast of the Iberian Peninsula, southern France and northern Italy, where the explained variance is at least 50 % ($>75\%$ for the Imperia, L'Estartit and Port Vendres tide gauges), RMS differences are below 4 cm and correlations are higher than 0.7. However, for the stations close to the Strait of Gibraltar the statistics are much poorer, e.g., the reconstructions can explain almost none of the variance of the original series. The results for Ibiza and Cagliari are not good either. In order to check whether the origin of the poor statistics of this band was due to a bad representation of the correlation matrix elements used 280 for the Optimal Interpolation, we also tested analytical correlation functions with different correlation characteristic lengths; however, no improvement in the results was achieved. This suggests that the stations showing poor statistics would have a sea level variability spatially decoupled from the others at this frequency band and/or there were problems with the observations.

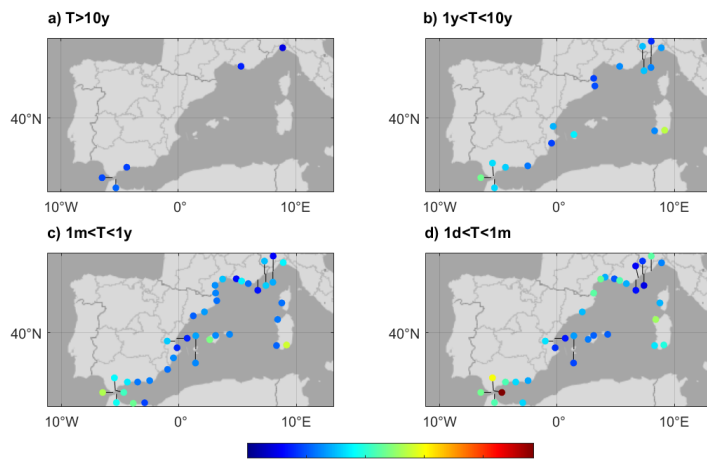
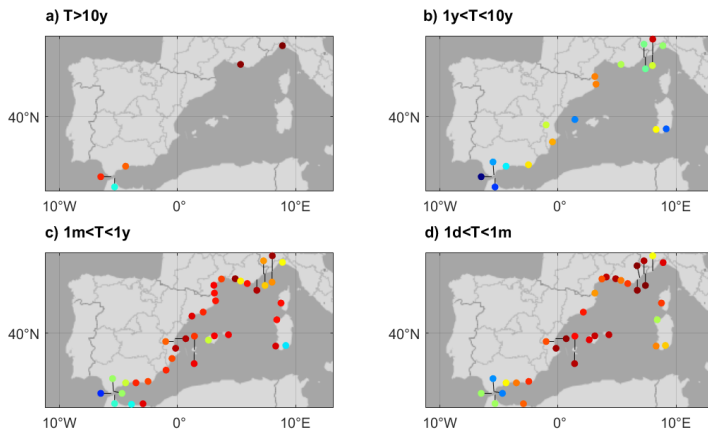


Figure 2: Results of the cross-validation test (I): RMS differences between the reconstructed values and the original series for the four frequency bands: a) $T > 10y$, b) $1y < T < 10y$, c) $1m > T > 1y$, d) $1d > T > 1m$.



In the intra-annual frequency band ($1m < T < 1y$) the statistics are better than for the previous band, with the worst values corresponding to the same stations: those located near the strait of Gibraltar, Ibiza and Cagliari. For the other stations, RMS
285 differences are below 3 cm, correlations above 0.8, and explained variances above 70 % in almost all cases.

Figure 3: Results of the cross-validation test (II): percentage of variance of the original tide gauge series explained by the reconstructions for the four frequency bands: a) $T > 10y$, b) $1y > T > 10y$, c) $1m > T > 1y$, d) $1d > T > 1m$.

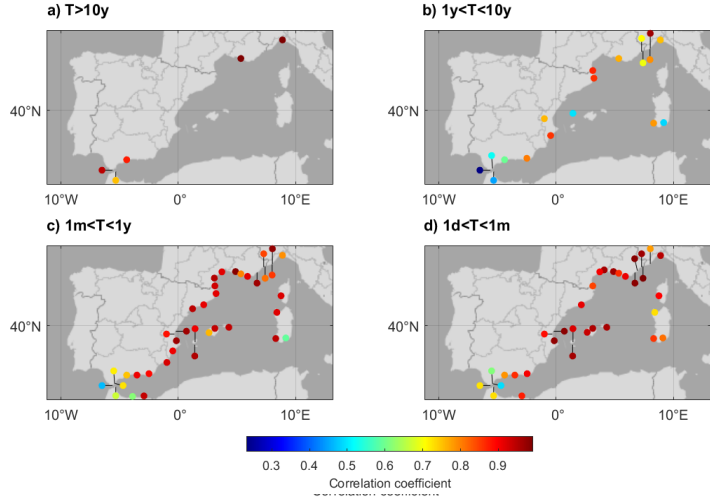


Figure 4: Results of the cross-validation test (III): correlation values between the reconstructed and the original tide gauge series for the four frequency bands: a) $T > 10y$, b) $1y > T > 10y$, c) $1m > T > 1y$, d) $1d > T > 1m$.

Finally, for the daily to monthly frequency band the statistics is also good, with RMS differences below 5 cm, correlations above 0.75, and explained variances above 60 % in almost all cases. The exceptions are Porto Torres and, again, the stations located near the strait of Gibraltar, where RMS differences almost reach 10 cm and the reconstruction explains less than 25 % of the original variance.

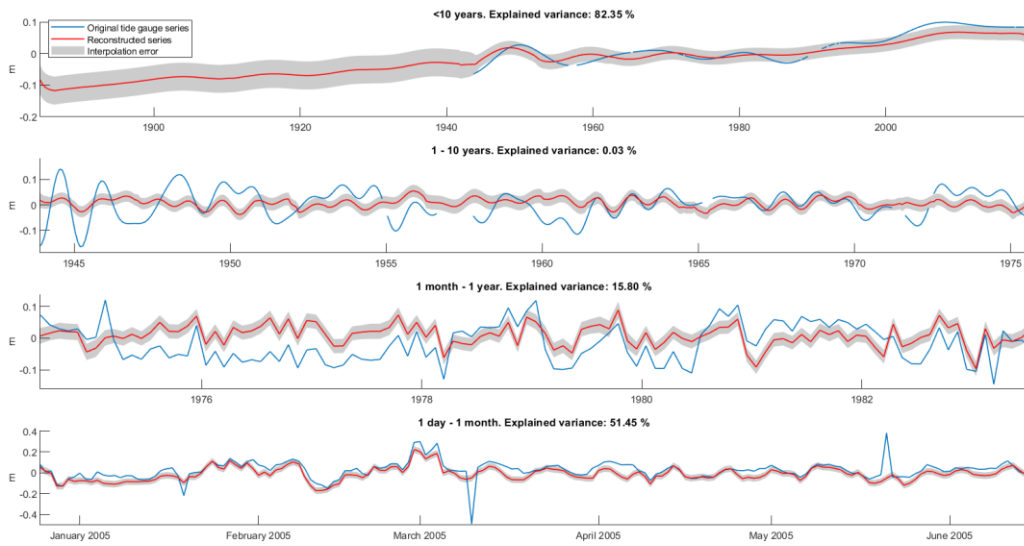


Figure 5: Comparison between the Tarifa tide gauge series and its reconstruction (for the four frequency bands), as given by the cross-validation test. The statistical interpolation error given by the Optimal Interpolation formulation (eq. (4)) is plotted in the form of an uncertainty for the interpolated values. Different time axes have been used for the different frequency bands, in order to correctly appreciate the variability of each band.

In order to visualize the bad results given by the cross-validation test near the strait of Gibraltar, we show a comparison between the original Tarifa tide gauge series and its reconstructions given by the cross-validation test for the four frequency bands (Fig. 5). Tarifa station was chosen because its series has been used for the reconstruction of all four frequency bands. The difficulties to reconstruct the original tide gauge series for the intra-annual and inter-annual frequency bands are well apparent. For these frequency bands, the differences between the original and the reconstructed series are larger than the statistical interpolation error given by the Optimal Interpolation formulation (Eq. (4)); this suggests that for some stations the correlation elements of the Optimal Interpolation matrices are not correctly represented. The plots also suggest that in some frequency bands the observations may have some problems that were not identified by the quality control. For instance, in the 1 day–1 month the explained variances are lowered by the spikes in the observations, which look unrealistic. Besides For comparison, Fig. 6 shows the same as Fig. 5 but for the Genoa station, which generally shows good statistics. As for Fig. 5, results are worse for the inter-annual and intra-annual bands (though notably better than in the case of Tarifa). This suggests that some of the coastal processes driving these frequency bands cannot be correctly interpolated by the reconstruction

method. On the other hand, in the daily to monthly frequency band the reconstruction is able to explain more than 88 % of the variance of the original series.

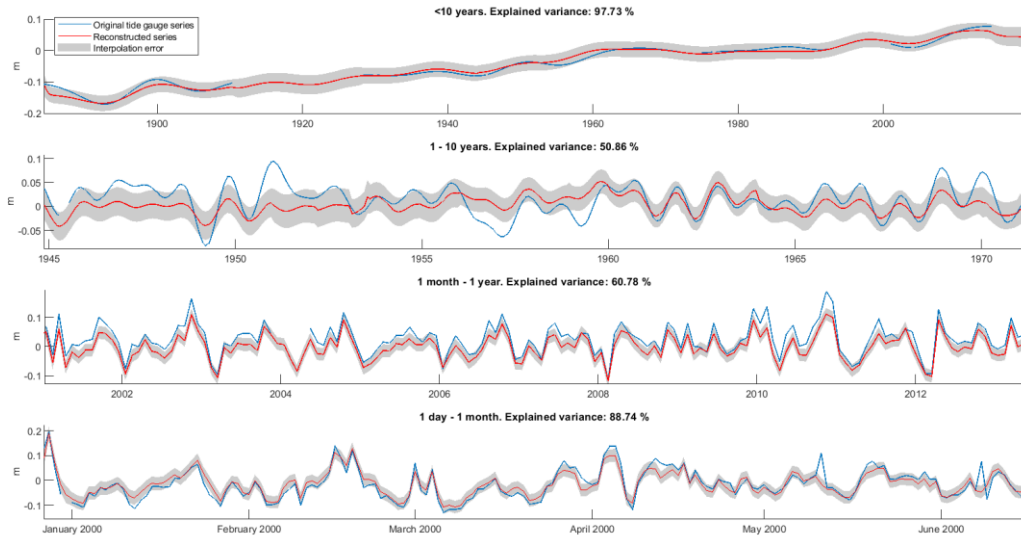


Figure 6: as for Figure 5, but for the Genoa tide gauge.

300 4.2 Merging of the reconstructed frequency bands

The cross-validation test has allowed some insight into the capabilities of the method. The next step was to obtain the main result of this work: the reconstructions for each frequency band, now considering all stations (that is, without withdrawing any station, as for the cross-validation test). After that, the reconstructions of the different bands were merged to evaluate the extent to which total sea level can be recovered, and hence to prove that the separation into frequency bands has been carried 305 out correctly.

As an example of the results, Fig. 7 shows, for the interpolation point closest to Barcelona tide gauge: i) the reconstructions in the four frequency bands; ii) a comparison between the original monthly series of Barcelona tide gauge and the merging of the three bands that correspond to periods $T>1m$; and iii) a comparison between the original daily series of Barcelona tide gauge and the merging of the four frequency bands, which corresponds to periods $T>1d$. In both cases 310 there is a high coincidence between the original and the merging of the reconstructed series, showing a correlation of 0.97 for the monthly case, and 0.99 for the daily case.

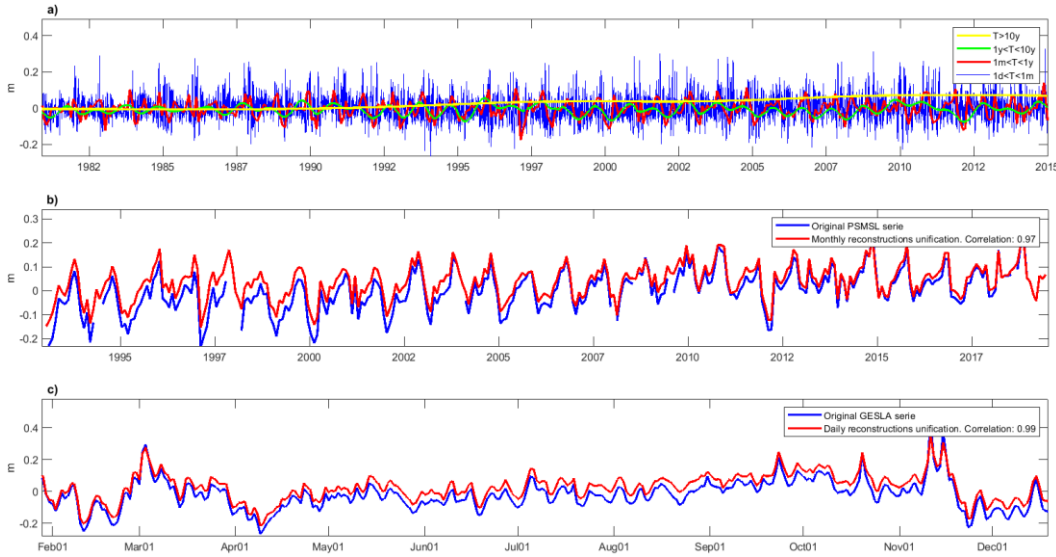


Figure 7: a) Reconstructions obtained in the four frequency bands for the interpolation point closest to Barcelona tide gauge. b) Monthly merging of the reconstructed frequency bands and the original monthly series of Barcelona tide gauge. c) Daily merging of the reconstructed frequency bands and the original daily series of Barcelona tide gauge. Different time intervals are shown for the monthly and daily series, in order to better appreciate the variability of the merged reconstructions and their differences with the original series.

Figure 8 shows the average interpolation errors of the merged series for the monthly case. Although it has been shown that in some stations actual errors can be higher than the theoretical error estimate, the latter can be useful to reflect the

315 spatial distribution of the interpolation accuracy. The quoted values are an average of the interpolation errors over the period from 1884 to 2019, since errors depend on the number of available stations, and this varies with time. The interpolation errors of the daily merged series are also quoted, in this case averaged over the period from 1980 to 2015. Maximum values of 5.26 cm are obtained for the monthly case, and of 7.05 cm for the daily case. The magnitude of the interpolation errors not only depends on the number of available stations, but also on their location with respect to the considered interpolation point.

320 For this reason, the spatial pattern of the errors clearly shows higher values in regions where no observations are available, such as the North African coast, or where tide gauge series are recent (and hence the average involves time periods when these stations were not available), such as in the Balearic archipelago for the monthly merging.

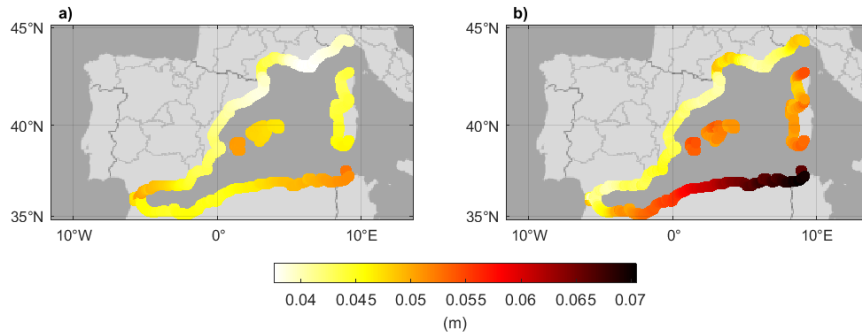


Figure 8: a) Average interpolation error for the monthly merging of the reconstructions. b) Average interpolation error for the daily merging of the reconstructions.

5 Analysis of the coastal sea level variability in the Western Mediterranean

325 5.1 Reconstructions trends

With the aim of characterising coastal sea level variability, some indicators were estimated from the obtained reconstructions. First, sea level trends were estimated for: i) the merged reconstructed series, for the period covered by altimetry (1993–2019); ii) tide gauge series spanning at least 80 % of that period; iii) altimetry series for the grid points closest to the coast. Trends were also calculated for the period (1884–2019). Figure 9 and Table 3 show all these trend

330 values.

For the period covered by altimetry, the trends of the reconstructions and of the altimetry series are similar in magnitude, with a basin-wide mean value of 2.70 ± 0.32 mm/year and 2.45 ± 0.49 mm/year, respectively. However, the values along the coast show a smoother continuity for the reconstruction than for altimetry. The heterogeneous coastal trend pattern obtained from altimetry does not seem to make physical sense and could be explained by the limitations of altimetry in coastal areas.

335 When compared with tide gauge trends computed for the period common to the three data sets (Table 3), a good agreement between tide gauges and the reconstruction is obtained except for Algeciras, Barcelona and Tarifa. The trends computed for these stations also show discrepancies with altimetric trends and even with the trends of nearby tide gauges. The lack of coherence between tide gauge trends in the Strait of Gibraltar has already been reported by different authors (e.g., Marcos and Tsimplis, 2008; Ross et al., 2000).

340 The main advantage of the reconstruction over tide gauges is that it allows the estimation of sea level trends along the entire coastline. Moreover, it does not have data gaps, which are responsible to significantly increase the uncertainty of the trends estimated from tide gauge series. The advantages of the reconstruction over altimetry are that it spans a longer period, provides more accurate results and smooths out eventual local anomalous trend values.

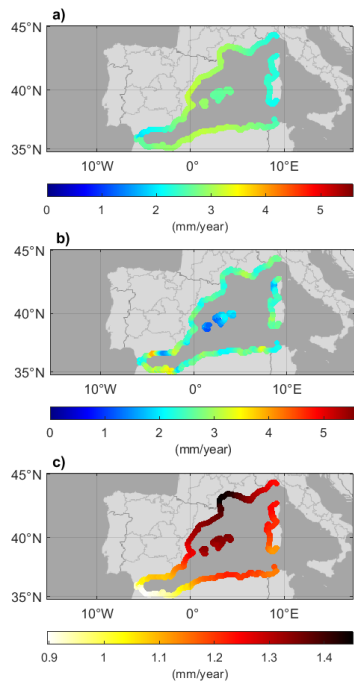


Figure 9: a) Sea level trends of the reconstructions for the period covered by altimetry (1993–2019). b) Sea level trends of the altimetry series at the points closest to the coast. c) Sea level trends calculated for the total period of the reconstructions (1884–2019), with a different colour scale.

345

For the total reconstruction period (1884–2019) the trends range from less than 1 mm/year in the African coasts close to Gibraltar to about 1.5 mm/year in the Gulf of Lions, with a regional mean value of 1.20 ± 0.14 mm/year. This result is consistent with the Mediterranean sea level trend computed from the three stations with the longest series, which is estimated to be between 1.1 and 1.3 mm/year (Gomis et al., 2012), as well as with the global rate of sea level rise for the 20th century, estimated through various reconstructions between 1.3 and 2 mm/year (Dangendorf et al., 2017). The trends show a rapid increase from the 1990s, coinciding with the period covered by altimetry with values ranging from 1.89 to 3.16 mm/yr. For that period the trends estimated from the reconstruction are coherent with those estimated by other authors (e.g. Bonaduce et al., 2016, obtained an average value for the whole Mediterranean basin of 2.44 ± 0.5 mm/y for the period 1993–2012).

355 **Table 3: Trends of the Tide Gauge, Reconstructions and Altimetry Series, for the Period Common to the Three Data Sets (1993–2019), with the Standard Deviations of the Linear Regression. Only the Stations whose Series are at least 80 % Complete have been included.**

Station	Tide gauge	Reconstruction	Altimetry
Algeciras	0.60 ± 0.48	2.10 ± 0.42	2.21 ± 0.36
Barcelona	5.59 ± 0.57	3.28 ± 0.52	2.86 ± 0.48
Ceuta	1.82 ± 0.41	2.51 ± 0.45	2.08 ± 0.35
L'Estartit	2.10 ± 0.51	2.97 ± 0.49	2.26 ± 0.37
Malaga	2.17 ± 0.50	2.26 ± 0.43	3.98 ± 0.39
Nice	2.85 ± 0.60	3.02 ± 0.56	2.70 ± 0.46
Sete	3.53 ± 0.64	3.09 ± 0.52	2.44 ± 0.42
Tarifa	4.32 ± 0.42	2.35 ± 0.44	2.43 ± 0.38
Toulon	3.05 ± 0.55	2.79 ± 0.54	3.39 ± 0.38
Valencia	4.16 ± 0.65	3.38 ± 0.54	2.37 ± 0.46

5.2 Sea level variability in different frequency bands

360 The seasonal cycle is one of the main components of sea level variability. Seasonal sea level changes are mainly caused by changes in the heat content of the upper layers of the ocean, and by changes in the atmospheric pressure field and winds that modulate the inflow of water from the Atlantic. In the Mediterranean sea, the seasonal cycle is estimated to account, on average, for 20 % of the variance of tide gauge series, and shows significant interannual variability. Also, seasonal cycle variations in coastal areas may differ significantly from those reported in the open ocean (Gomis et al., 2012; Woodworth et al., 2019). The seasonal cycle of the coastal reconstructions, estimated from monthly mean values, accounts on average for 24 % of the coastal sea level variance.

365 Figure 10 shows the patterns of the variability in different frequency bands quantified in terms of the standard deviation. For the seasonal cycle the variability ranges between 2.92 and 4.97 cm, with a smooth variation along the coast. The largest standard deviations are found at the Eastern coast of the Iberian Peninsula, in agreement with previous authors that located 370 the maximum annual sea level cycle of the western Mediterranean in Alicante (Marcos and Tsimplis, 2007b) and the maximum annual cycle of the atmospheric contribution to sea level in the Alborán Sea (Gomis et al., 2008). The subtraction of the seasonal cycle does not lead to a large reduction of the standard deviation of the reconstruction, which on average is 1 cm lower without the seasonal cycle. The deseasoned reconstruction has an average standard deviation of 3.77 cm for periods $T > 1$ y, 4.91 cm for periods $1 \text{m} < T < 1$ y and 4.27 cm for periods $1 \text{d} < T < 1 \text{m}$. In all frequency bands, the highest standard 375 deviations of the deseasoned series are obtained in the Gulf of Lion.

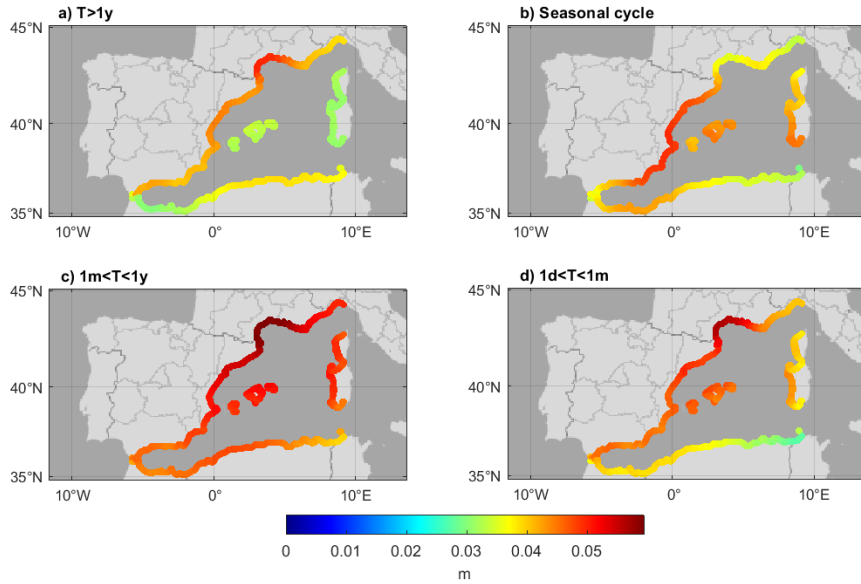


Figure 10: a) Standard deviation of the reconstructions for the band $T>1y$, with the seasonal cycle subtracted. b) Standard deviation of the seasonal cycle adjusted from the reconstructions. c) Standard deviation of the reconstructions for the band $1m < T < 1y$, with the seasonal cycle subtracted. d) Standard deviation of the reconstructions for the band $1d < T < 1m$, with the seasonal cycle subtracted.

5.3 Influence of atmospheric climate modes on sea level variability

The four main atmospheric modes driving western Mediterranean sea level variability are NAO, EA, EA/WR and SCAN.

Their influence has already been studied among others by Martínez-Asensio et al. (2014), who used long tide gauge series from the whole basin, as well as altimetry products. Our coastal reconstructions allow us to complement the study of the

380 influence of these climate modes in two ways: first, by covering the entire coastal region (i.e., not only where tide gauge records are available), and second, avoiding the use of coastal altimetry. In addition, the sea level series of our reconstructions cover a longer period than altimetric products, thus enabling the analysis to extend to the whole period covered by climate indices (since 1950).

Figure 11 shows the correlation patterns between the monthly coastal reconstruction and the four climate indices. 385 Correlations have been calculated both for the complete series, and for the seasonal mean values of the reconstruction and the indices, with winter accounting for January–March, spring for April–June, summer for July–September and autumn for October–December.

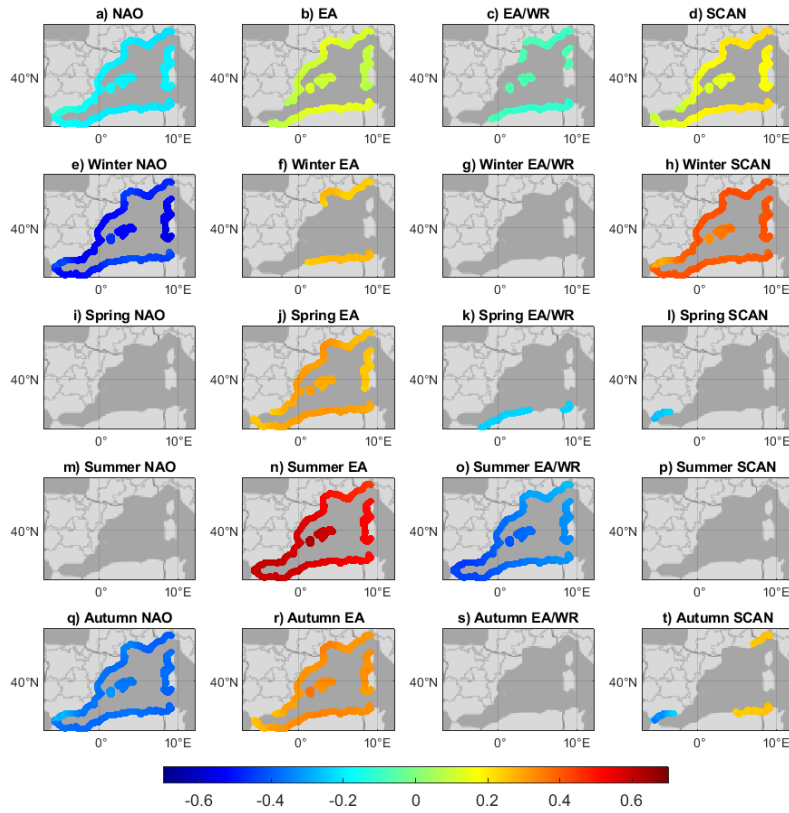


Figure 11: Seasonal and total maps of correlation coefficients between climate indices and the coastal sea level reconstruction for the period 1950–2019. Only correlations significant at the 95 % level have been plotted.

For the total series, the NAO index is anti-correlated with sea level since the western Mediterranean participates of the
 390 subtropical high pressures and hence sea level lowers when the NAO index is in a positive phase. Conversely, the EA and SCAN indices show a positive correlation. In winter, two indices dominate sea level variability: the NAO index, with correlation values below -0.6 at some points and showing significant correlations along the entire basin coastline, and the SCAN index, with positive correlations (the NAO and SCAN indices are interdependent and anti-correlated with each other). The obtained correlation patterns are similar to those obtained from open-ocean altimetry for the period 1993–2010
 395 (Martínez-Asensio et al., 2014), although the values obtained for the coastal reconstructions are somewhat weaker for the

two dominant indices. In spring, the EA index clearly dominates over the others, being the only one with significant correlations throughout the basin, with positive correlation values above 0.3.

In summer, the correlation patterns obtained from our reconstructions slightly differ from those obtained from tide gauge series in the western Mediterranean by Martínez-Asensio et al. (2014). Our results show that, during summer, the EA is the 400 dominating index, with positive correlations up to 0.5 basin-wide, while the EA/WR index shows negative correlations of around -0.3. Martínez-Asensio et al. (2014) also obtain positive correlations between the tide gauges and the EA index, but always lower than 0.5, and often not significant; for the EA/WR index they obtain non-significant negative correlations. Overall, the sea level reconstruction suggests a greater influence of the EA and EA/WR indices (mainly related to freshwater 405 and heat fluxes) on western Mediterranean sea level variability in summer than what is obtained from pointwise observations. Finally, in autumn it is the NAO index that seems to dominate the variability, with correlations around -0.5, followed by EA, with values up to 0.4.

6 Discussion

A major objective of this work was to explore whether using tide gauge data in an optimal way could result in a coastal sea level dataset more accurate than current coastal altimetry products. Figure 12 shows, for the different frequency bands, the 410 correlations between the daily reconstructions resulting from the cross-validation test (i.e., withdrawing from the input observations the tide gauge record that is intended to be reproduced) and the original tide gauge series, as well as the correlations between altimetry (at the closest grid point to the tide gauge) with the DAC applied, and the original tide gauge series. Correlations have been computed for the period covered by both altimetry and our reconstructions, that is, from 1993 to 2015.

415 Figure 12 shows that the correlations are in general significantly higher for the reconstructed series than for the corrected altimetry for all frequency bands. It should be kept in mind that these correlations have been calculated for the period (the last decades) when a larger number of observations in all bands are available (this also explains why the correlations shown in Fig.12 are higher than those shown in Fig. 4 for the whole period of the reconstruction). Namely, the correlations between the reconstructions obtained through the cross-validation test and the tide gauge series are higher than 0.5 at all stations and 420 frequencies, being higher than 0.75 in most of the stations. Conversely, for altimetry with the DAC applied and for the frequency band for which it performs better ($1d < T < 1m$), correlations are all lower than 0.5 (for the other frequency bands correlations are much lower). It is worth mentioning that in this band the results are better because the variability in that frequency is dominated by the atmospheric mechanical forcing, which is reasonably well modelled by DAC. More precisely, the average correlations between coastal reconstructions and tide gauges are 0.95 for the $T > 10y$ band, 0.83 for the $1y < T < 10y$ 425 band, 0.92 for the $1m < T < 1y$ band, and 0.91 for the $1d < T < 1m$ band. On the other hand, the average correlations between the altimetry series with the applied DAC and the tide gauge series are -0.25 for the $T > 10y$ band, 0.08 for the $1y < T < 10y$ band, 0.02 for the $1m < T < 1y$ band, and 0.43 for the $1d < T < 1m$ band. This confirms that using tide gauge data in an optimal way allows the retrieval of coastal sea level with a significantly higher accuracy than using altimetric products for all time scales.

Tabla con formato

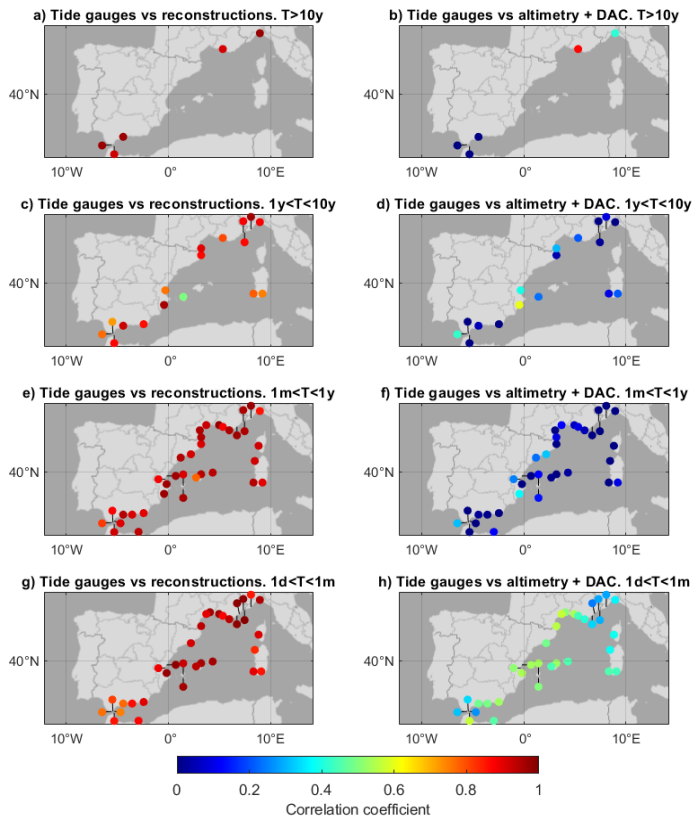


Figure 12: Correlations between the reconstructions obtained through the cross-validation test and the original tide gauge series (left), and correlations between the atmospherically corrected altimetry series and the original tide gauge series (right), for the four frequency bands.

The proposed method to estimate coastal sea level can be applied in a straightforward way to any other region, keeping in mind two potential limitations. The first one is that the correlation elements of the Optimal Interpolation matrices should be reliable, and this implies the existence of a reliable, long enough sea level data with high spatio-temporal resolution, such as the outputs of the SOCIB model in our case. Otherwise, the correlation matrices will have to be calculated through the fitting of analytical functions, which is usually less accurate. The second limitation is that the quality of the reconstruction will also depend on the spatial distribution of tide gauge observations. A relevant advantage of the method is that given the spatial distribution of tide gauges, the interpolation errors can be estimated a priori. Although the theoretical error estimate may be

optimistic (due to the assumption that the correlation matrix elements are fully representative of actual correlations), it usually provides a reliable error pattern. Moreover, having in mind that the theoretical interpolation error constitutes a lower boundary for actual errors can be useful to decide about the application or not of the method.

Regarding previous efforts to retrieve sea level in the region, all previous reconstructions gave greater emphasis to the open ocean and have the limitation of relying on altimetric products when coastal sea level is attempted to be reproduced. To our knowledge, this is the first attempt to obtain a reconstruction specific to the coastal region.

7 Conclusions

Sea level reconstructions have been obtained for the whole coast of the western Mediterranean basin by applying an Optimal Interpolation scheme to tide gauge observations. The reconstructions have been obtained for four frequency bands, and then merged to obtain total sea level. In order to validate the robustness of the method, a cross-validation test was applied using the tide gauge series themselves as independent observations. The test was applied to each frequency band, giving successful results except at a few particular stations (e.g., near the Strait of Gibraltar). It was also checked that the merging of the reconstructions obtained in the four frequency bands accurately recovers the original total sea level series at coastal points close to tide gauges.

A major conclusion of the work is that the reconstructions provide significantly better estimates of coastal sea level than current altimetry products with the atmospheric correction added back. This has been proved again via cross-validation, by obtaining the reconstruction nearby each tide gauge location with a prior withdrawal of that tide gauge record from the interpolation scheme.

The reconstructions have been used to gain some insight in different aspects of coastal sea level variability. Thus, coastal trend values have been calculated for the period (1884–2019). Also, trends computed for the period covered by altimetry are fairly consistent with those obtained from altimetry data, but the pattern of the trends along the coast shows a smoother continuity for the reconstructions. It has also been found that the relationship of sea level and climate indices obtained by Martínez-Asensio et al. (2014) are generally comparable with those obtained from our reconstructions, but they show noticeable discrepancies in summer (the signs of the correlations with the EA and EA/WR indices are inverted) likely due to the type of sea level product used by Martínez-Asensio et al. (2014).

In summary, results indicate that it is possible to obtain accurate coast-wide sea level series from an optimal processing of tide gauge observations only. The accuracy of the reconstruction has been shown to vary regionally. The level of accuracy depends on the number of available stations and also on the accuracy of the representation of the correlation elements of the Optimal Interpolation matrices which in our case are provided by a numerical model. The applicability and performance of the method to other regions is conditioned, first, by the availability of long enough sea level datasets with the required spatiotemporal resolution to compute reliable correlation functions, and second, to the number of available tide gauge observations and their spatial distribution.

470 **Appendix A: Validation of the correlations inferred from SOCIB model outputs for the optimal interpolation of
coastal sea level**

In order to validate the use of the correlations of the numerical model outputs in the implementation of the optimal interpolation, gaussian noise was added to the model series, whose variance was adjusted to carry out a first reconstruction test using these series as pseudo-observations, to verify the ability of the reconstruction method. The differences between the correlation patterns between the tide gauge series and correlation patterns between the model series with noise (for the points 475 closest to the tide gauges) have been included in this document.

Figures A1, A2 and A3 show the differences between the correlations between pairs of tide gauges and the correlations between pairs of SOCIB model series located at the closest point to each tide gauge. Gaussian noise has been added to the model series, with an error variance being optimised to minimise the differences with respect to tide gauge correlations for each frequency band. Correlations that could not be calculated due to the shortness of the time period spanned by the two 480 series are shown in black.

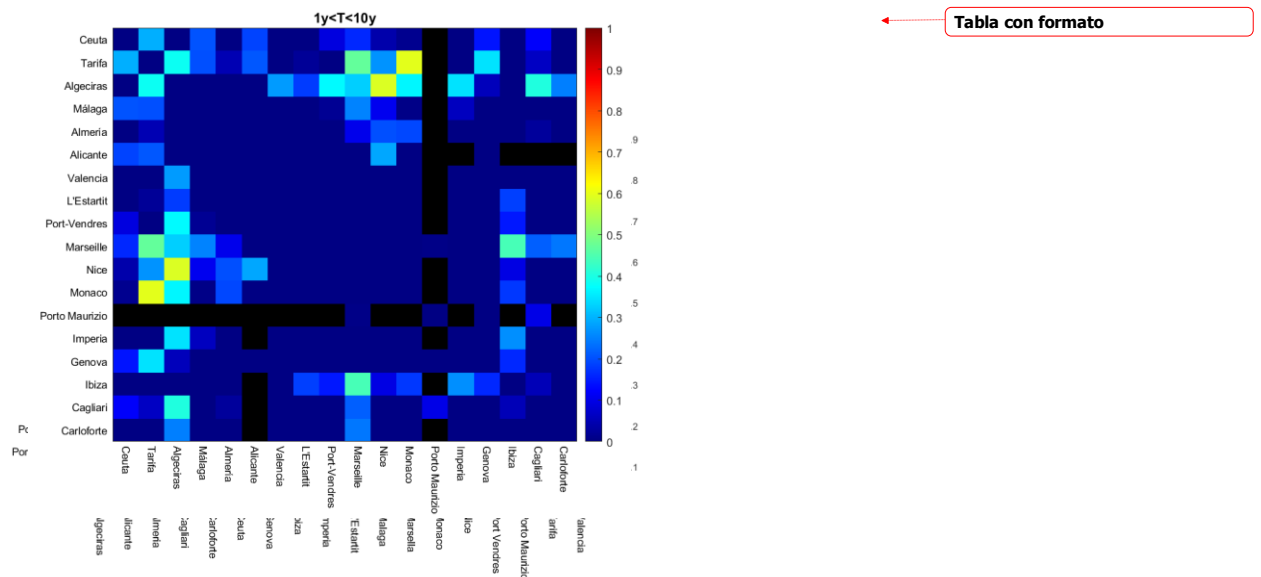


Figure A1: Differences between the correlation between tide gauge series and the correlation between SOCIB model series (with random noise added) at the points closest to each tide gauge, for the frequency band $1y < T < 10y$.

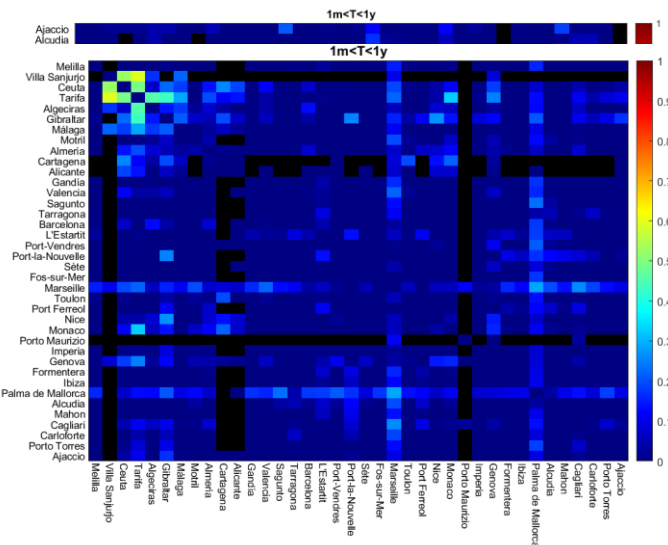


Figure A2: Differences between the correlation between tide gauge series and the correlation between SOCIB model series (with random noise added) at the points closest to each tide gauge, for the frequency band $1m < T < 1y$.

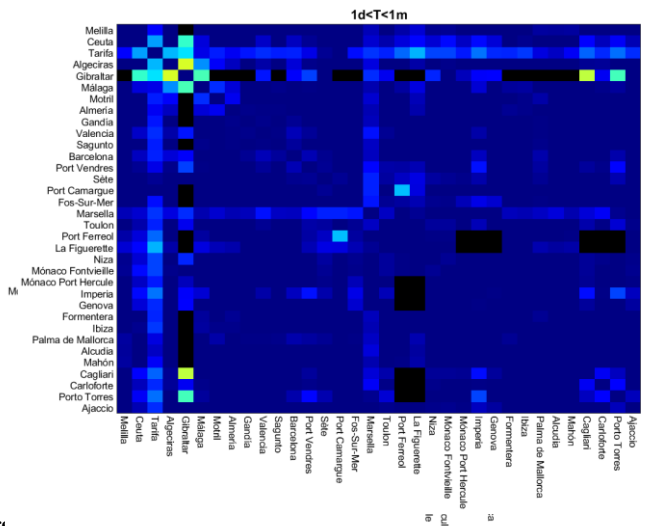


Figure A3: Differences between the correlation between tide gauge series and the correlation between SOCIB model series (with random noise added) at the points closest to each tide gauge, for the frequency band $1d < T < 1m$.

Appendix B: Statistical interpolation errors associated to the reconstruction of each frequency band

485 Statistical interpolation errors associated to the reconstruction of the four frequency bands are shown in Figure B1. The displayed values are the average of the errors along the period spanned by the reconstruction, since errors vary with time due to the variation of the number of tide gauge series available. The spatial distributions of the errors indicate that these are larger in areas where no observations are available, or where tide gauge series are shorter.

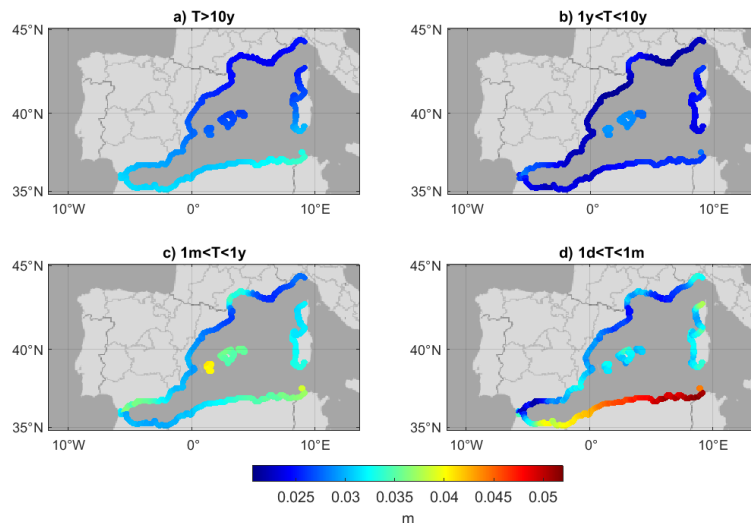


Figure B1: Temporal average of the analysis error (in m) (a) for the band $T > 10y$ (b) for the band $1y < T < 10y$, (c) for the band $1m < T < 1y$ and (d) for the band $1d < T < 1m$.

490

Data availability. The coastal sea level reconstructions data for the western Mediterranean Basin developed in this work are available at PANGAEA Data Publisher at <https://doi.pangaea.de/10.1594/PANGAEA.945345>. Tide gauge data are available from Global Extreme Sea Level Analysis project (<http://www.gesla.org/>; Caldwell et al., 2015; Haigh et al., 2021; Woodworth et al., 2016), and from the Permanent Service for Mean Sea Level (PSMSL; <https://www.psmsl.org/>). WMOP 495 numerical model outputs are available through the Balearic Islands Coastal Observing and Forecasting System data center (SOCIB; <https://www.socib.es/?seccion=dataCenter>). The satellite altimetry data are available through the Copernicus Marine Environment Monitoring Service (CMEMS, <https://marine.copernicus.eu/es>, product identifier: SEALEVEL_MED_PHY_L4 REP_OBSERVATIONS_008_051, last accessed on 6 May 2021 and now included as part of the SEALEVEL_EUR_PHY_L4_MY_008_068), and the Dynamic Atmospheric Correction data are available through the 500 Archiving, Validation and Interpretation of Satellite Oceanographic (AVISO;

<https://www.aviso.altimetry.fr/en/data/products/auxiliary-products/dynamic-atmospheric-correction/description-atmospheric-corrections.html>). The Climatic indices data are available through the NOAA Climate Prediction Centre website (<http://www.cpc.ncep.noaa.gov/data/teledoc/telecontents.shtml>).

505 *Author Contribution.* DG and GJ conceived the study. JR analysed the entire dataset, did the computational work, and wrote the first draft of the manuscript. DG and GJ developed most of the methodology and devised the structure of the article. All authors contributed to the interpretation of the results, and to the final version of the manuscript.

510 *Competing interests.* The authors declare that they have no conflict of interest.

510 *Acknowledgments.* The authors acknowledge financial support from MCIN/ERDF through project VENOM (PGC2018-099285-B-C21, PGC2018-099285-B-C22) and from MCIN and European Union through project UNCHAIN (PCI2019-103680/ AEI / 10.13039/501100011033). We thank J. Villalonga and M. Agulles for their comments and computational help.

515 *Financial support.* Grant VENOM (PGC2018-099285-B-C21, PGC2018-099285-B-C22) funded by MCIN/AEI/10.13039/501100011033 and by ERDF A way of making Europe. Grant UNCHAIN (PCI2019-103680/ AEI / 10.13039/501100011033), funded by MCIN/AEI/10.13039/501100011033 and by the European Union.

References

520 Bonaduce, A., Pinardi, N., Oddo, P., Spada, G., and Larnicol, G.: Sea-level variability in the Mediterranean Sea from altimetry and tide gauges, *Clim. Dynam.*, 47, 2851–2866, <https://doi.org/10.1007/s00382-016-3001-2>, 2016.

Bretherton, F. P., Davis, R. E., and Fandry, C. B.: A technique for objective analysis and design of oceanographic experiments applied to MODE-73*, *Deep Sea Research and Oceanographic Abstracts*, 23, 559–582, [https://doi.org/https://doi.org/10.1016/0011-7471\(76\)90001-2](https://doi.org/https://doi.org/10.1016/0011-7471(76)90001-2), 1976.

525 Bueh, C. and Nakamura, H.: Scandinavian pattern and its climatic impact, *Q. J. Roy. Meteor. Soc.*, 133, 2117–2131, <https://doi.org/10.1002/qj.173>, 2007.

Calafat, F. M. and Gomis, D.: Reconstruction of Mediterranean sea level fields for the period 1945–2000, *Global Planet. Change*, 66, 225–234, <https://doi.org/10.1016/j.gloplacha.2008.12.015>, 2009.

Carrère, L. and Lyard, F.: Modeling the barotropic response of the global ocean to atmospheric wind and pressure forcing - 530 comparisons with observations, *Geophys. Res. Lett.*, 30, <https://doi.org/10.1029/2002GL016473>, 2003.

Cazenave, A., Palanisamy, H., and Ablain, M.: Contemporary sea level changes from satellite altimetry: What have we learned? What are the new challenges?, *Adv. Space Res.*, 62, 1639–1653, <https://doi.org/10.1016/j.asr.2018.07.017>, 2018.

Cipollini, P., Calafat, F. M., Jevrejeva, S., Melet, A., and Prandi, P.: Monitoring Sea Level in the Coastal Zone with Satellite Altimetry and Tide Gauges, Springer, Cham, 35–59, https://doi.org/10.1007/978-3-319-56490-6_3, 2017.

535 le Cozannet, G., Nicholls, R. J., Hinkel, J., Sweet, W. v., McInnes, K. L., van de Wal, R. S. W., Slanger, A. B. A., Lowe, J. A., and White, K. D.: Sea level change and coastal climate services: The way forward, *Journal of Marine Science and Engineering*, 5, <https://doi.org/10.3390/jmse5040049>, 2017.

Dangendorf, S., Marcos, M., Wöppelmann, G., Conrad, C. P., Frederikse, T., and Riva, R.: Reassessment of 20th century global mean sea level rise, *P. Natl. Acad. Sci. USA*, 114, 5946–5951, <https://doi.org/10.1073/pnas.1616007114>, 2017.

540 Douglas, B. C.: Sea Level Change in the Era of the Recording Tide Gauge, in: *Sea Level Rise: History and Consequences*, vol. 75, edited by: Douglas, B. C., Kearney, M. S., and Leatherman, S. P., Academic Press, 37–64, [https://doi.org/https://doi.org/10.1016/S0074-6142\(01\)80006-1](https://doi.org/https://doi.org/10.1016/S0074-6142(01)80006-1), 2001.

FitzGerald, D. M., Fenster, M. S., Argow, B. A., and Buynevich, I. v.: Coastal impacts due to sea-level rise, *Annu. Rev. Earth Pl. Sc.*, 36, 601–647, <https://doi.org/10.1146/annurev.earth.35.031306.140139>, 2008.

545 Gomis, D. and Pedder, M. A.: Errors in dynamical fields inferred from oceanographic cruise data: Part I. The impact of observation errors and the sampling distribution, *J. Marine Syst.*, 56, 317–333, <https://doi.org/10.1016/j.jmarsys.2005.02.002>, 2005.

Gomis, D., Ruiz, S., Sotillo, M. G., Álvarez-Fanjul, E., and Terradas, J.: Low frequency Mediterranean sea level variability: The contribution of atmospheric pressure and wind, *Global Planet. Change*, 63, 550 <https://doi.org/10.1016/j.gloplacha.2008.06.005>, 2008.

Gomis, D., Tsimplis, M., Marcos, M., Fenoglio-Marc, L., Pérez, B., Raicich, F., Vilíbić, I., Wöppelmann, G., and Monserrat, S.: Mediterranean Sea Level Variability and trends, in: *The climate of the Mediterranean region: From the past to the future*, edited by: Lionello, P., Elsevier, 257–299, 2012.

Hasselmann, S., Lionello, P., and Hasselmann, K.: An optimal interpolation scheme for the assimilation of spectral wave data, *J. Geophys. Res.-Oceans*, 102, 15823–15836, <https://doi.org/10.1029/96JC03453>, 1997.

555 Hastie, T., Tibshirani, R., and Friedman, J.: *Model Assessment and Selection*, in: *The Elements of Statistical Learning. Data Mining, Inference, and Prediction*, Springer Series in Statistics, 219–260, 2008.

Holgate, S. J. and Woodworth, P. L.: Evidence for enhanced coastal sea level rise during the 1990s, *Geophys. Res. Lett.*, 31, <https://doi.org/10.1029/2004GL019626>, 2004.

560 Holgate, S. J., Matthews, A., Woodworth, P. L., Rickards, L. J., Tamisiea, M. E., Bradshaw, E., Foden, P. R., Gordon, K. M., Jevrejeva, S., and Pugh, J.: New data systems and products at the permanent service for mean sea level, *J. Coastal Res.*, 29, 493–504, <https://doi.org/10.2112/JCOASTRES-D-12-00175.1>, 2013.

Jordà, G., Gomis, D., and Álvarez-Fanjul, E.: The VANI2-ERA hindcast of sea-level residuals: atmospheric forcing of sea-level variability in the Mediterranean Sea (1958–2008), *Sci. Mar.*, 133–146, <https://doi.org/10.3989/scimar.03612.19C>, 565 2012.

Josey, S. A., Somot, S., and Tsimplis, M.: Impacts of atmospheric modes of variability on Mediterranean Sea surface heat exchange, *J. Geophys. Res.-Oceans*, 116, <https://doi.org/10.1029/2010JC006685>, 2011.

Juza, M., Mourre, B., Renault, L., Górnara, S., Sebastián, K., Lora, S., Beltran, J. P., Frontera, B., Garau, B., Troupin, C., Torner, M., Heslop, E., Casas, B., Escudier, R., Vizoso, G., and Tintoré, J.: SOCIB operational ocean forecasting system and multi-platform validation in the western mediterranean sea, *J. Oper. Oceanogr.*, 9, s155–s166, <https://doi.org/10.1080/1755876X.2015.1117764>, 2016.

Kaplan, A., Kushnir, Y., Cane, M. A., and Blumenthal, M. B.: Reduced space optimal analysis for historical data sets: 136 years of Atlantic sea surface temperatures, *J. Geophys. Res.-Oceans*, 102, 27835–27860, <https://doi.org/10.1029/97JC01734>, 1997.

Kirwan, M. L., Guntenspergen, G. R., D'Alpaos, A., Morris, J. T., Mudd, S. M., and Temmerman, S.: Limits on the adaptability of coastal marshes to rising sea level, *Geophys. Res. Lett.*, 37, <https://doi.org/10.1029/2010GL045489>, 2010.

Lyu, K., Zhang, X., Church, J. A., Slanger, A. B. A., and Hu, J.: Time of emergence for regional sea-level change, *Nat. Clim. Change*, 4, 1006–1010, <https://doi.org/10.1038/nclimate2397>, 2014.

Marcos, M. and Tsimplis, M. N.: Forcing of coastal sea level rise patterns in the North Atlantic and the Mediterranean Sea, *Geophys. Res. Lett.*, 34, <https://doi.org/10.1029/2007GL030641>, 2007a.

Marcos, M. and Tsimplis, M. N.: Variations of the seasonal sea level cycle in southern Europe, *J. Geophys. Res.-Oceans*, 112, <https://doi.org/10.1029/2006JC004049>, 2007b.

Marcos, M. and Tsimplis, M. N.: Coastal sea level trends in Southern Europe, *Geophys. J. Int.*, 175, 70–82, <https://doi.org/10.1111/j.1365-246X.2008.03892.x>, 2008.

Marcos, M., Wöppelmann, G., Matthews, A., Ponte, R. M., Birol, F., Arduin, F., Coco, G., Santamaría-Gómez, A., Ballu, V., Testut, L., Chambers, D., and Stopa, J. E.: Coastal Sea Level and Related Fields from Existing Observing Systems, *Surv. Geophys.*, 40, 1293–1317, <https://doi.org/10.1007/s10712-019-09513-3>, 2019.

Martínez-Asensio, A., Marcos, M., Tsimplis, M. N., Gomis, D., Josey, S., and Jordà, G.: Impact of the atmospheric climate modes on Mediterranean sea level variability, *Global Planet. Change*, 118, 1–15, <https://doi.org/10.1016/j.gloplacha.2014.03.007>, 2014.

Meyssignac, B., Calafat, F. M., Somot, S., Rupolo, V., Stocchi, P., Llovel, W., and Cazenave, A.: Two-dimensional reconstruction of the Mediterranean sea level over 1970–2006 from tide gauge data and regional ocean circulation model outputs, *Global Planet. Change*, 77, 49–61, <https://doi.org/10.1016/j.gloplacha.2011.03.002>, 2011.

Pedder, M. A.: Interpolation and Filtering of Spacial Observations Using Successive Corrections and Gaussian Filters, *Mon. Weather Rev.*, 121, 2889–2902, [https://doi.org/10.1175/1520-0493\(1993\)121<2889:IAFOSO>2.0.CO;2](https://doi.org/10.1175/1520-0493(1993)121<2889:IAFOSO>2.0.CO;2), 1993.

Pejic, D. and Arsic, M.: Minimization and Maximization of Functions: Golden-Section Search in One Dimension, in: Exploring the DataFlow Supercomputing Paradigm. Computer Communications and Networks, edited by: Milutinovic, V. and Kotlar, M., Springer, Cham, 55–90, https://doi.org/10.1007/978-3-030-13803-5_3, 2019.

Piccioni, G., Dettmering, D., Bosch, W., and Seitz, F.: TICON: Tidal CONstants based on GESLA sea-level records from globally located tide gauges, *Geosci. Data J.*, 6, 97–104, <https://doi.org/10.1002/gdj3.72>, 2019.

Pozzi, F., di Matteo, T., and Aste, T.: Exponential smoothing weighted correlations, *Eur. Phys. J. B*, 85, <https://doi.org/10.1140/epjb/e2012-20697-x>, 2012.

Rasmussen, C. E.: Evaluation of gaussian processes and other methods for non-linear regression, Ph.D. thesis, University of 605 Toronto, 1996.

Ross, T., Garrett, C., and Traon, P. Y. le: Western Mediterranean sea-level rise: Changing exchange flow through the strait of Gibraltar, *Geophys. Res. Lett.*, 27, 2949–2952, <https://doi.org/10.1029/2000GL011653>, 2000.

von Schuckmann, K., le Traon, P. Y., Smith, N., Pascual, A., Brasseur, P., Fennel, K., Djavidnia, S., Aaboe, S., Fanjul, E., 610 Autret, E., Axell, L., Aznar, R., Benincasa, M., Bentamy, A., Boberg, F., Bourdallé-Badie, R., Nardelli, B. B., Brando, V. E., Bricaud, C., Breivik, L. A., Brewin, R. J. W., Capet, A., Ceschin, A., Ciliberti, S., Cossarini, G., de Alfonso, M., de Pascual Collar, A., de Kloe, J., Deshayes, J., Desportes, C., Drévillon, M., Drillet, Y., Droghei, R., Dubois, C., Embury, O., Etienne, H., Fratianni, C., Lafuente, J. G., Sotillo, M. G., Garric, G., Gasparin, F., Gerin, R., Good, S., Gourrion, J., Grégoire, M., Greiner, E., Guinehut, S., Gutknecht, E., Hernandez, F., Hernandez, O., Hoyer, J., Jackson, L., Jandt, S., Josey, S., Juza, M., Kennedy, J., Kokkini, Z., Korres, G., Kouts, M., Lagemaa, P., Lavergne, T., le Cann, B., Legeais, J., 615 Lemieux-Dudon, B., Levier, B., Lien, V., Maljutenko, I., Manzano, F., Marcos, M., Marinova, V., Masina, S., Mauri, E., Mayer, M., Melet, A., Mélin, F., Meyssignac, B., Monier, M., Müller, M., Mulet, S., Naranjo, C., Notarstefano, G., Paulmier, A., Gomez, B. P., Pérez Gonzalez, I., Peneva, E., Perruche, C., Peterson, K. A., Pinardi, N., Pisano, A., Pardo, S., Poulain, P. M., Raj, R. P., Raudsepp, U., Ravdas, M., Reid, R., Rio, M. H., Salon, S., Samuelsen, A., Sammartino, M., et al.: Copernicus Marine Service Ocean State Report, *J. Oper. Oceanogr.*, 11, S1–S142, 620 <https://doi.org/10.1080/1755876X.2018.1489208>, 2018.

Shchepetkin, A. F. and McWilliams, J. C.: The regional oceanic modeling system (ROMS): A split-explicit, free-surface, topography-following-coordinate oceanic model, *Ocean Model.*, 9, 347–404, <https://doi.org/10.1016/j.ocemod.2004.08.002>, 2005.

Spalding, M. D., Ruffo, S., Lacambra, C., Meliane, I., Hale, L. Z., Shepard, C. C., and Beck, M. W.: The role of ecosystems 625 in coastal protection: Adapting to climate change and coastal hazards, *Ocean and Coastal Management*, 90, 50–57, <https://doi.org/10.1016/j.ocemcoaman.2013.09.007>, 2014.

Tsimplis, M. N. and Shaw, A. G. P.: Seasonal sea level extremes in the Mediterranean Sea and at the Atlantic European coasts, *Nat. Hazard. Earth Sys.*, 10, 1457–1475, <https://doi.org/10.5194/nhess-10-1457-2010>, 2010.

Tsimplis, M. N., Shaw, A. G. P., Pascual, A., Marcos, M., Pasaric, M., and Fenoglio-Marc, L.: Can we reconstruct the 630 20th century sea level variability in the Mediterranean Sea on the basis of recent altimetric measurements?, in: *Remote Sensing of the European Seas*, edited by: Barale, V. and Gade, M., Springer, 307–318, 2008.

Vignudelli, S., Birol, F., Benveniste, J., Fu, L. L., Picot, N., Raynal, M., and Roinard, H.: Satellite Altimetry Measurements of Sea Level in the Coastal Zone, *Surv. Geophys.*, 40, 1319–1349, <https://doi.org/10.1007/s10712-019-09569-1>, 2019.

Wolff, C., Vafeidis, A., Muis, S., Lincke, D., Satta, A., Lionello, P., Jimenez, J. A., Conte, D., and Hinkel, J.: A
635 Mediterranean coastal database for assessing the impacts of sea-level rise and associated hazards, *Scientific Data*, 5,
<https://doi.org/10.1038/sdata.2018.44>, 2018.

Woodworth, P., Melet, A., Marcos, M., Ray, R. D., Wöppelmann, G., Sasaki, Y. N., Cirano, M., Hibbert, A., Huthnance, J.
M., Monserrat, S., and Merrifield, M. A.: Forcing Factors Affecting Sea Level Changes at the Coast, *Sur. in Geophys.*, 40,
1351–1397, <https://doi.org/10.1007/s10712-019-09531-1>, 2019.

640 Woodworth, P. L., Hunter, J. R., Marcos, M., Caldwell, P., Menéndez, M., and Haigh, I.: Towards a global higher-frequency
sea level dataset, *Geosci. Data J.*, 3, 50–59, <https://doi.org/10.1002/gdj3.42>, 2016.